











# Supplementary Material

## Understanding the Dynamics of DNNs Using Graph Modularity

Yao Lu<sup>1</sup> , Wen Yang<sup>1</sup> , Yunzhe Zhang<sup>1</sup> , Zuohui Chen<sup>1</sup> , Jinyin Chen<sup>1</sup> ,  
Qi Xuan<sup>1</sup>  , Zhen Wang<sup>2</sup>  , and Xiaoni Yang<sup>1,3</sup> 

<sup>1</sup> Institute of Cyberspace Security, Zhejiang University of Technology, Hangzhou, 310023. China

{yaolu.zjut,czuohui}@gmail.com, {chenjinyin,xuanqi}@zjut.edu.cn,  
wenyang.zjut@outlook.com, xsgxlz@live.cn

<sup>2</sup> School of Artificial Intelligence, Optics and Electronics (iOPEN), Northwestern Polytechnical University, Xi'an 710072. China

zhenwang0@gmail.com

<sup>3</sup> Science and Technology on Communication Information Security Control  
Laboratory, Jiaxing 314033, China  
yxn2117@126.com

This document supplements our paper by providing additional experiments and experimental details.

## A Supplementary Experiments

### A.1 Different Similarity indexes to Calculate the Similarity Matrix

In this subsection, we replace cosine similarity with pearson correlation coefficient to calculate the similarity matrix. We can observe from Fig. B1 that the modularity curves are almost the same as those in the manuscript, demonstrating that various similarity indexes can be utilized to obtain the modularity.

### A.2 Modularity curves of Randomly Initialized Models

Having observed the upward trend of modularity emerging in pre-trained models, we next study whether this phenomenon exists in randomly initialized models. Hence, we conduct experiments with VGG16 and ResNet18 on CIFAR-10. In Fig. B2, we show the modularity curves of randomly initialized models. Since the randomly initialized models can not learn useful feature representations, the connections among samples at each layer are completely random. Thus, the modularity nearly maintains constant in the randomly initialized models compared to pre-trained models.

### A.3 Ablation of $k$

In Fig.7(b), the variability of  $k$  is small, it is reasonable to question whether  $k$  has a significant impact when  $k$  is large ( $k \gg 11$ ). To answer this doubt, we

set  $N = 500$ ,  $k = 100, 200, 300, 400$  to repeat the experiment. Fig. B3 shows the result, from which we find that different values of  $k$  have a certain impact on modularity values but do not hurt the tendency of modularity curves. When  $k$  is large, each node connects many unrelated nodes (i.e., nodes belonging to different communities), which weakens the intra-community connections but strengthens the inter-community connections, resulting in a decrease in the modularity value.

## B Implementation Details

### B.1 ImageNet50

The 50 classes we randomly selected from ImageNet [49] are shown as follows, you can also build the dataset yourself.

n01443537 goldfish, *Carassius auratus*  
n01484850 great white shark, white shark, man-eater, man-eating shark, *Carcharodon carcharias*  
n01491361 tiger shark, *Galeocerdo cuvieri*  
n01494475 hammerhead, hammerhead shark  
n01496331 electric ray, crampfish, numbfish, torpedo  
n01498041 stingray  
n01514668 cock  
n01514859 hen  
n01518878 ostrich, *Struthio camelus*  
n01530575 brambling, *Fringilla montifringilla*  
n01531178 goldfinch, *Carduelis carduelis*  
n01532829 house finch, linnet, *Carpodacus mexicanus*  
n01534433 junco, snowbird  
n01537544 indigo bunting, indigo finch, indigo bird, *Passerina cyanea*  
n01558993 robin, American robin, *Turdus migratorius*  
n01560419 bulbul  
n01580077 jay  
n01582220 magpie  
n01592084 chickadee  
n01601694 water ouzel, dipper  
n01608432 kite  
n01614925 bald eagle, American eagle, *Haliaeetus leucocephalus*  
n01616318 vulture  
n01632777 axolotl, mud puppy, *Ambystoma mexicanum*  
n01667778 terrapin  
n01688243 frilled lizard, *Chlamydosaurus kingi*  
n01728920 ringneck snake, ring-necked snake, ring snake  
n01773157 black and gold garden spider, *Argiope aurantia*  
n01795545 black grouse  
n01847000 drake  
n07768694 pomegranate

n07802026 hay  
 n07831146 carbonara  
 n07836838 chocolate sauce, chocolate syrup  
 n07860988 dough  
 n07871810 meat loaf, meatloaf  
 n07873807 pizza, pizza pie  
 n09193705 alp  
 n09229709 bubble  
 n09246464 cliff, drop, drop-off  
 n09256479 coral reef  
 n09288635 geyser  
 n09332890 lakeside, lakeshore  
 n09399592 promontory, headland, head, foreland  
 n09421951 sandbar, sand bar  
 n09428293 seashore, coast, seacoast, sea-coast  
 n09468604 valley, vale  
 n09472597 volcano  
 n09835506 ballplayer, baseball player  
 n10148035 groom, bridegroom

## B.2 Statistics of Models

The statistics of pre-trained models used in this paper are shown in Table B1. Moreover, in order to better investigate the redundant layers in models. We design a series of variants. The model structures of these variants are shown in Table B2-B5.

**Table B1.** The statistics of pre-trained models.

Dataset	VGGs				ResNets				
	V11	V13	V16	V19	R18	R34	R50	R101	R152
CIFAR-10	92.11%	93.68%	93.63%	93.36%	94.78%	95.14%	95.38%	95.18%	95.32%
CIFAR-100	66.87%	70.19%	72.34%	72.63%	76.87%	76.69%	78.03%	78.21%	78.64%
ImageNet50	83.97%	85.87%	85.04%	87.32%	82.55%	82.99%	85.04%	87.32%	87.89%

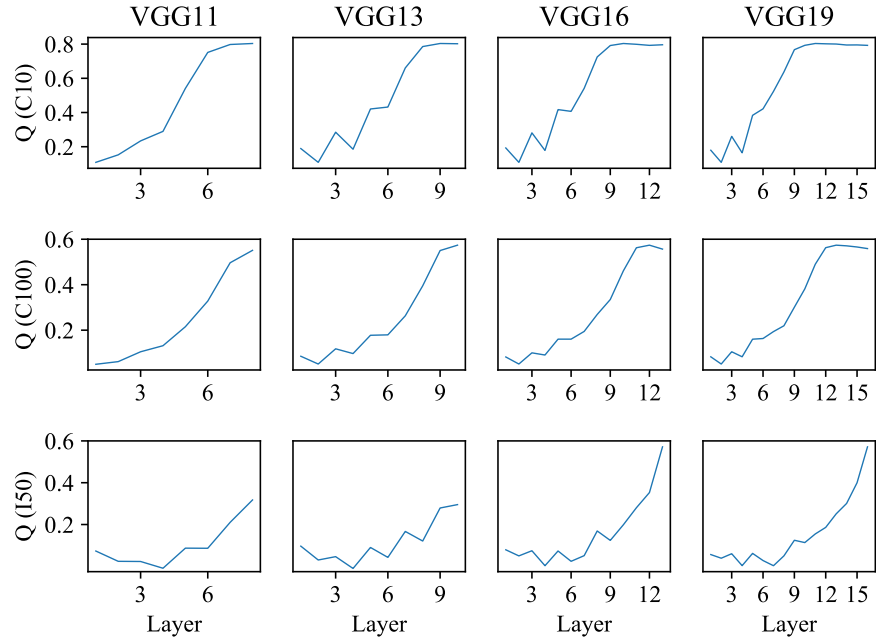


**Fig. B1.** We utilize pearson correlation coefficient instead of cosine similarity to calculate the similarity matrix. We can find the modularity curves are almost same as those in the main text, which demonstrates that our modularity can be obtained by various indexes.

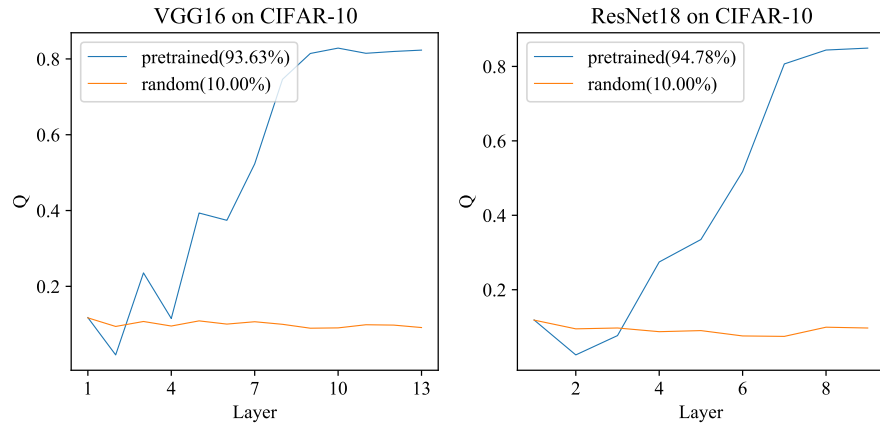


**Fig. B2.** Modularity curves of well-optimized and randomly initialized models.

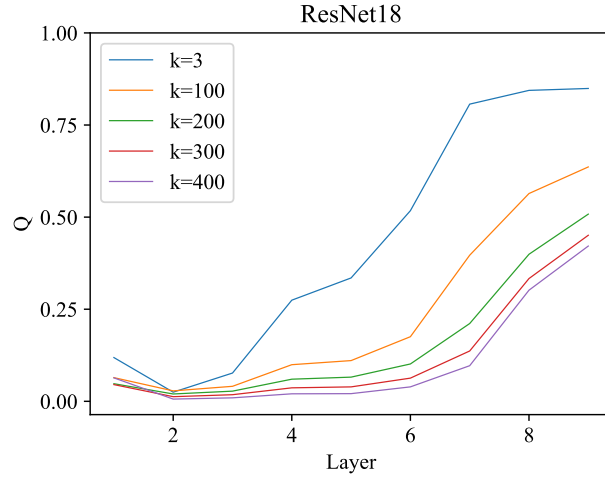


**Fig. B3.** The influence of k on the modularity when k is large.

**Table B2.** The model structures of variants of VGG19 on CIFAR-10.

VGG19.6	VGG19.5	VGG19.4	VGG19.3	VGG19.2	VGG19.1	VGG19
input (32 × 32 RGB images)						
conv3-64	conv3-64	conv3-64	conv3-64	conv3-64	conv3-64	conv3-64
conv3-64	conv3-64	conv3-64	conv3-64	conv3-64	conv3-64	conv3-64
maxpool						
conv3-128	conv3-128	conv3-128	conv3-128	conv3-128	conv3-128	conv3-128
conv3-128	conv3-128	conv3-128	conv3-128	conv3-128	conv3-128	conv3-128
maxpool						
conv3-256	conv3-256	conv3-256	conv3-256	conv3-256	conv3-256	conv3-256
conv3-256	conv3-256	conv3-256	conv3-256	conv3-256	conv3-256	conv3-256
conv3-256	conv3-256	conv3-256	conv3-256	conv3-256	conv3-256	conv3-256
conv3-256	conv3-256	conv3-256	conv3-256	conv3-256	conv3-256	conv3-256
maxpool						
conv3-512	conv3-512	conv3-512	conv3-512	conv3-512	conv3-512	conv3-512
conv3-512	conv3-512	conv3-512	conv3-512	conv3-512	conv3-512	conv3-512
conv3-512	conv3-512	conv3-512	conv3-512	conv3-512	conv3-512	conv3-512
conv3-512	conv3-512	conv3-512	conv3-512	conv3-512	conv3-512	conv3-512
maxpool						
conv3-512	conv3-512	conv3-512	conv3-512	conv3-512	conv3-512	conv3-512
conv3-512	conv3-512	conv3-512	conv3-512	conv3-512	conv3-512	conv3-512
conv3-512	conv3-512	conv3-512	conv3-512	conv3-512	conv3-512	conv3-512
maxpool						
FC-512						
FC-512						
FC-10						
soft-max						

**Table B3.** The model structures of variants of ResNet152 on CIFAR-10.

Layer	Size	Res152_30	Res152_26	Res152_21	Res152_16	Res152_11	Res152_5	
conv1	32×32	3×3, 64, stride 1						
conv2_x	32×32	1×1, 64 3×3, 64 1×1, 256	1×1, 64 3×3, 64 1×1, 256	1×1, 64 3×3, 64 1×1, 256	1×1, 64 3×3, 64 1×1, 256	1×1, 64 3×3, 64 1×1, 256	1×1, 64 3×3, 64 1×1, 256	3
conv3_x	16×16	1×1, 128 3×3, 128 1×1, 512	1×1, 128 3×3, 128 1×1, 512	1×1, 128 3×3, 128 1×1, 512	1×1, 128 3×3, 128 1×1, 512	1×1, 128 3×3, 128 1×1, 512	1×1, 128 3×3, 128 1×1, 512	8
conv4_x	8×8	1×1, 256 3×3, 256 1×1, 1024	1×1, 256 3×3, 256 1×1, 1024	1×1, 256 3×3, 256 1×1, 1024	1×1, 256 3×3, 256 1×1, 1024	1×1, 256 3×3, 256 1×1, 1024	1×1, 256 3×3, 256 1×1, 1024	31
conv5_x	4×4	1×1, 512 3×3, 512 1×1, 2048	1×1, 512 3×3, 512 1×1, 2048	1×1, 512 3×3, 512 1×1, 2048	1×1, 512 3×3, 512 1×1, 2048	1×1, 512 3×3, 512 1×1, 2048	1×1, 512 3×3, 512 1×1, 2048	3
	1×1	adaptive average pool, 10-d fc, softmax						

**Table B4.** The model structures of variants of ResNet152 on ImageNet50.

Layer	Size	Res152_30	Res152_26	Res152_21	Res152_16	Res152_11	Res152_5	
conv1	112×112	7×7, 64, stride 2						
conv2_x	56×56	3×3 max pool, stride 2						
		1×1, 64 3×3, 64 1×1, 256	1×1, 64 3×3, 64 1×1, 256	1×1, 64 3×3, 64 1×1, 256	1×1, 64 3×3, 64 1×1, 256	1×1, 64 3×3, 64 1×1, 256	1×1, 64 3×3, 64 1×1, 256	3
conv3_x	28×28	1×1, 128 3×3, 128 1×1, 512	1×1, 128 3×3, 128 1×1, 512	1×1, 128 3×3, 128 1×1, 512	1×1, 128 3×3, 128 1×1, 512	1×1, 128 3×3, 128 1×1, 512	1×1, 128 3×3, 128 1×1, 512	8
conv4_x	14×14	1×1, 256 3×3, 256 1×1, 1024	1×1, 256 3×3, 256 1×1, 1024	1×1, 256 3×3, 256 1×1, 1024	1×1, 256 3×3, 256 1×1, 1024	1×1, 256 3×3, 256 1×1, 1024	1×1, 256 3×3, 256 1×1, 1024	31
conv5_x	7×7	1×1, 512 3×3, 512 1×1, 2048	1×1, 512 3×3, 512 1×1, 2048	1×1, 512 3×3, 512 1×1, 2048	1×1, 512 3×3, 512 1×1, 2048	1×1, 512 3×3, 512 1×1, 2048	1×1, 512 3×3, 512 1×1, 2048	3
	1×1	adaptive average pool, 50-d fc, softmax						

**Table B5.** The model structures of variants of VGG11 on CIFAR-10 and CIFAR-100.

VGG11.3	VGG11.2	VGG11.1	VGG11
input ( $32 \times 32$ RGB images)			
conv3-64	conv3-64	conv3-64	conv3-64
maxpool			
conv3-128	conv3-128	conv3-128	conv3-128
maxpool			
conv3-256	conv3-256	conv3-256	conv3-256
	conv3-256	conv3-256	conv3-256
maxpool			
conv3-512	conv3-512	conv3-512	conv3-512
		conv3-512	conv3-512
maxpool			
conv3-512	conv3-512	conv3-512	conv3-512
			conv3-512
maxpool			
FC-512			
FC-512			
FC-10			
soft-max			